J. Fluid Mech. (2020), *vol*. 905, A3. © The Author(s), 2020.
Published by Cambridge University Press
doi:10.1017/jfm.2020.693

Anisotropic scaling lengths of colloidal monolayers near a water–air interface

Na Li[1,2,†], Wei Zhang[3], Zehui Jiang[4] and Wei Chen[1,†]

[1]State Key Laboratory of Physics and Department of Physics, Fudan University, Shanghai 200433, PR China

[2]College of Information and Communication, National University of Defense Technology, Xian, PR China

[3]School of Materials and Physics, China University of Mining and Technology, Xuzhou 221116, PR China

[4]Department of Physics, Harbin Institute of Technology, Harbin 150001, PR China

(Received 12 February 2020; revised 16 June 2020; accepted 11 August 2020)

Near-interface colloidal monolayers are often used as model systems for research on hydrodynamics in biophysics systems and in the chemical industry. Using microrheological methods, the correlated diffusion of particles is experimentally measured in colloidal monolayers near a water–air interface. The results show that the scaling lengths ($\chi_{||}$, $\chi_{\perp}$) of such colloidal monolayers are anisotropic in two orthogonal directions within the monolayer, which are parallel and perpendicular to the line connecting the centres of a particle pair. The former ($\chi_{||}$) is the Saffman length of the monolayer, while the latter ($\chi_{\perp}$) is a function of both the Saffman length and the radius of the colloids. The size of the colloids is involved in $\chi_{\perp}$ but not $\chi_{||}$, which reflects the discrete nature of the monolayer in the transverse direction and the continuous nature of the monolayer in the longitudinal direction. From the scaling lengths, the viscosities of the colloidal monolayers are obtained, which agree with those obtained from the single-particle diffusion coefficients. The influence of the boundary condition imposed by the nearby interface on the hydrodynamic interactions is in a power-law behaviour of the distance z.

Key words: colloids, thin films, microfluidics

1. Introduction

The characterization of the viscoelastic properties of colloidal suspensions has long been the subject of fundamental research due to the ubiquity of such suspensions in biology and industry. Microrheological techniques have been widely employed for such measurements due to their advantages in probing the local material response in systems such as porous media (Cai, Panyukov & Rubinstein 2011; Di Rienzo e*t al.* 2014; Wang *et al.* 2014; Begam *et al.* 2015), biological systems (Ramadurai *et al.* 2009; Parigi *et al.* 2014; He *et al.* 2016) and microfluidic devices (McWhirter, Noguchi & Gompper 2009; Frydel & Diamant 2010; Shani *et al.* 2014; Misiunas *et al.* 2015; Huang et al. 2017). Research has shown that the viscoelastic properties of a colloidal suspension are strongly affected by the confining boundaries (Caruso *et al.* 1991; Ouali & Pefferkorn 1996; Dufresne *et al.* 2000;

† Email addresses for correspondence: phchenwei@fudan.edu.cn, lina919@yeah.net

Wille *et al.* 2002; Cui *et al.* 2004; Wang *et al.* 2009; Oppenheimer & Diamant 2010; Huang & Szlufarska 2015). Two-dimensional (2-D) colloidal monolayers have traditionally been used to model the dynamic behaviours of proteins and other large molecules near a biomembrane (Saffman & Delbrück 1975; Wang *et al.* 2009, 2011*a*; Park & Lee 2015; He *et al.* 2016). The hydrodynamic mechanisms in a colloidal monolayer differ from those in a 3-D bulk liquid or a 2-D liquid film (Di Leonardo *et al.* 2008; Oppenheimer & Diamant 2009, 2010; Vivek & Weeks 2015). The mass of such a 2-D monolayer is conserved within the monolayer, and momentum can propagate between the monolayer and the surrounding 3-D liquid (Oppenheimer & Diamant 2009, 2010). To characterize the hydrodynamic interactions (HIs) between the particles in such a confined quasi-2-D system, a characteristic length should be introduced. For a continuous two-fluid system, Saffman (Saffman & Delbrück 1975; Saffman 1976) defined this characteristic length as $\lambda_s = \eta^{(s)}/\eta^{(b)}$, where $\eta^{(s)}$ is the surface viscosity of the liquid membrane and $\eta^{(b)}$ is the bulk viscosity of the surrounding liquid. When the distance r between two particles is much smaller than λ_s, the momentum is conserved in the 2-D membrane. When the distance r is much larger than λ_s, the momentum diffuses into the surrounding 3-D liquid (Saffman & Delbrück 1975; Saffman 1976; Prasad, Koehler & Weeks 2006; Zhang *et al.* 2013*a*,*b*).

In Saffman's model, the stress (momentum flux) in the membrane is spatially isotropic and decays logarithmically as $\sim \log(1/r)$ (Saffman & Delbrück 1975; Saffman 1976) due to the conservation of momentum in the 2-D liquid (Vivek & Weeks 2015). The characteristic length in Saffman's model is solely characterized by λ_s. The work of Weeks *et al.* (Prasad *et al.* 2006) experimentally validated that λ_s serves as a scaling length in a system consisting of a large-molecule membrane at a water–air interface. Zhang *et al.* (2013*b*) also noted that the scaling length in a particle monolayer at a water–air interface depends on both the particle size and the Saffman length. Previous work (Saffman & Delbrück 1975; Saffman 1976; Prasad *et al.* 2006; Oppenheimer & Diamant 2009, 2010; Zhang *et al.* 2013*b*) has mainly focused on the HIs in a liquid film suspended in a bulk liquid or at a liquid–liquid interface. In contrast, few experimental studies have investigated the dynamic features of particle monolayers close to a liquid–air interface, which are distinctly different from those for a monolayer at the interface. Knowledge of the transitions of the HIs from the 2-D monolayer to the 3-D bulk liquid is essential to understand the role played by the interface in the HIs in the monolayer.

In this study, we report experimental investigations of the correlated diffusion of colloidal particles in a monolayer close to a water–air interface. In a water–oil system, the correlated diffusion of particles was found independent on z, the distance between monolayer and the interface (Zhang et al. 2013*a*). This was in contrast to the intuitive expectation: the mechanism of HIs near a boundary should be sensitive to the distance away from the boundary. We thought that, due to the high viscosity of oil, the strength of HIs through oil phase is much higher than that of HIs through the water film between the monolayer and the interface, which results in the independence of the correlated diffusion on the thickness of the water film z. To verify this, we set up a water–air system, where the water film plays an important role in HIs between particles and contributes significantly to the correlated diffusion of colloidal particles since the viscosity of air can be ignored. And we do obtain quantitative results on the z-dependent correlated diffusion, and the universal behaviours of such correlated diffusion have been studied here. The results show that the scaling lengths in the longitudinal and transverse directions are different. In the longitudinal direction, the scaling length is the Saffman length λ_s. In the transverse direction, the scaling length is a function of λ_s and the particle radius a. With these scaling lengths, the curves describing the correlated diffusion of particles under

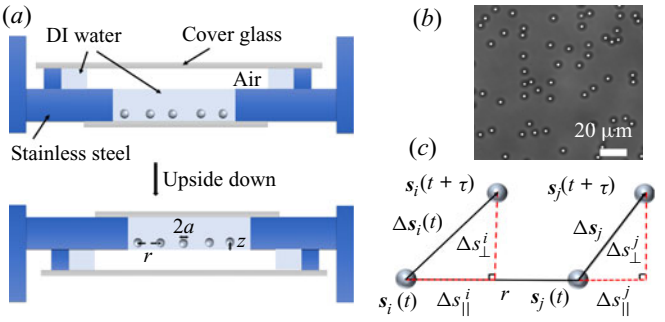

FIGURE 1. Schematic view of the experiment. (*a*) Schematic view of the system. (*b*) Optical microscope image of silica particles ($a = 1.57$ μm) suspended near a water–air interface at an area fraction of $n = 0.04$. (*c*) The definitions of $\Delta s_{||}$, $\Delta s_\perp$ and $\Delta \boldsymbol{s}_i(\tau)$.

different conditions can be collapsed into one master curve. Using these scaling factors, the viscosity of such a monolayer can be estimated, and the result is consistent with that obtained from one-particle measurements.

2. Experimental method

Samples of three kinds of colloidal particles were obtained from Bangs Laboratories, namely, silica spheres with radii of $a = 1.57$ μm (Si1), 1.0 μm (Si2) and 0.6 μm (Si3). The particle samples were cleaned 8–10 times via centrifugation prior to use to scour off the surfactant in the solution. Then, the cleaned particles were suspended in deionized water to form preparatory samples. The deionized (DI) water was produced using a Synergy UV System from Millipore. The sample cell was made of stainless steel and had a structure similar to that in Zhang *et al.* (2013*a*). The cell consisted of a solution tank at the bottom and an air tank at the top. The inner diameter of the solution tank was 8.3 mm. The depth of both tanks was 0.8 mm. A preparatory sample was introduced into the solution tank until the sample solution bulged. The extra solution was removed using a glass straw. The opening of the straw was half-immersed at the solution surface. When the extra solution was sucked off by the straw, the possible impurities on the interface were also removed. After the prepared cell was sealed with a coverslip, the sealed cell was placed upside down and left undisturbed for 7–8 h. Then, the particles settled down toward the water–air interface under gravity. The surface tension of the water was sufficiently strong to retain the water on the top side of the cell. A stable particle monolayer stays close to the water–air interface due to the interaction of the image charge of the particles. The separation between the water–air interface and the centres of particles in the monolayer is denoted by z. The experimental system is shown in figure 1(*a*). A microscope (Olympus X71 with 60× objectives, NA 0.70) and a CCD camera (Prosilica GE1050, 1024 pixels × 1024 pixels, 17 fps) were used to record sequences of images of the particles in the monolayer (figure 1*b*). Each sequence comprised 500 frames. The image resolution of the camera was 0.09 μm pix^{-1}. The closest particles in adjacent frames were identified as the same particle. The particle trajectories $\boldsymbol{s}(t)$ were obtained using our homemade particle tracking program.

3. Results

The single-particle self-diffusion coefficient $D_s(n)$ can be obtained from the mean square particle displacement $\langle \Delta \boldsymbol{s}_i^2(\tau) \rangle = 4D_s(n)\tau$, where $\Delta \boldsymbol{s}_i(\tau) = \boldsymbol{s}_i(t+\tau) - \boldsymbol{s}_i(t)$, as

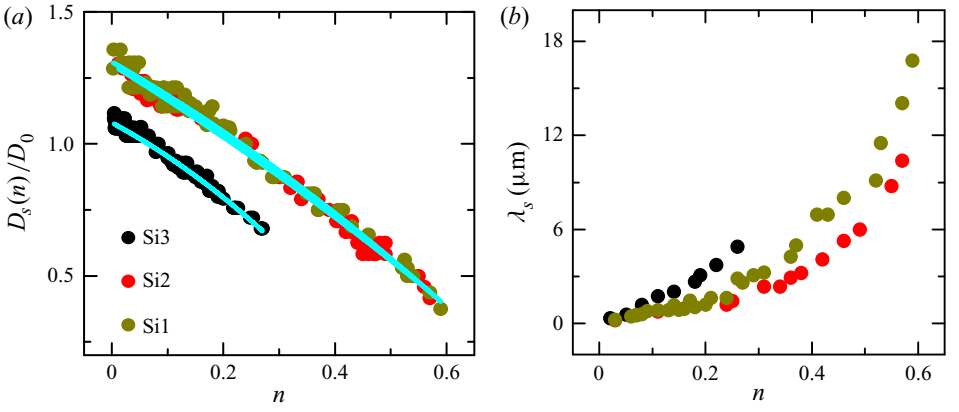

FIGURE 2. (*a*) Normalized self-diffusion coefficients of a single particle. The normalized self-diffusion coefficient $D_s(n)/D_0$ is plotted as a function of the area fraction n for samples Si1, Si2 and Si3. The solid lines represent the second-order polynomial fits to the formula $D_s(n)/D_0 = \alpha(1 - \beta n - \gamma n^2)$ for each sample. (*b*) The dependence of the Saffman length λ_s of monolayers on the area fraction n for each sample.

shown in figure 1(*c*). Here, τ is the lag time, and n is the area fraction of the particles. Figure 2(*a*) shows the normalized curves of $D_s(n)/D_0$ as functions of the particle concentration n for the three samples, where D_0 is the diffusion coefficient for a single particle in the bulk water, $D_0 = k_BT/6\pi\eta^{(b)}a$. The value for each data point in figure 2(*a*) was obtained by averaging more than 10^6 particles. The solid lines in figure 2(*a*) illustrate the results of fitting the data to $D_s(n)/D_0 = \alpha(1 - \beta n - \gamma n^2)$ (Chen & Tong 2008). When $n \to 0, D_s(0)/D_0 = \alpha$, where $D_s(0)$ is the single-particle diffusion coefficient in the monolayer in the dilute limit. The fitted values of the parameters α, β and γ for the three samples are given in table 1. As seen from this table, a larger particle size corresponds to a larger value of α and a smaller value of β. Here, the value of the parameter α reflects the strength of the viscosity experienced by a single particle in the local environment in the dilute solution limit. A large α implies a low viscosity (Zhang *et al.* 2013*a*). The value of the parameter β represents the strength of the effective hydrodynamic interactions between two particles, excluding the effects of the local environment. A large β reflects strong hydrodynamic interactions. The value of the parameter γ represents the strength of the many-body effect among the particles in the monolayer.

The separation z is calculated according to (3.1) (Wang *et al.* 2009, 2011*b*):

$$\frac{D_s(0)}{D_0} = 1 + \frac{3}{16}\left(\frac{2\eta^{(b)} - 3\eta^{(a)}}{\eta^{(b)} + \eta^{(a)}}\right)\left(\frac{a}{z}\right), \tag{3.1}$$

where $\eta^{(b)}$ is the viscosity of the bulk water, $\eta^{(a)}$ is the viscosity of the air and z is the separation between the particle centre and the liquid interface. The calculated values of z are shown in table 1. It should be noted that the thermal motion of the particles prevents them from staying at a fixed location, and rather causes them to sway around their equilibrium positions, while their vertical positions follow a Boltzmann distribution. The measured value of z presented here is an average one, with a fluctuation width Δz in the order of $k_BT/\Delta mg$, where Δm is the difference of the mass between the particle and a water sphere with the same size. This is true for a 1 μm radius silica particle, $\Delta z \sim 0.1$ μm, for example. All our measurements are the results of HIs averaged in the

https://doi.org/10.1017/jfm.2020.693 Published online by Cambridge University Press

Sample	a (μm)	α	β	γ	z (μm)	z/a	$\kappa^{(0)}$	$\kappa^{(1)}$	$[\eta]$
Si1	1.57	1.31 ± 0.03	0.92 ± 0.05	0.4 ± 0.1	1.89 ± 0.05	1.21 ± 0.03	15.3 ± 0.4	3.55 ± 0.05	1.27 ± 0.05
Si2	1.00	1.30 ± 0.03	1.00 ± 0.05	0.3 ± 0.1	1.26 ± 0.05	1.26 ± 0.05	15.4 ± 0.4	3.47 ± 0.07	1.31 ± 0.05
Si3	0.60	1.08 ± 0.02	1.05 ± 0.05	1.3 ± 0.3	2.81 ± 0.04	4.68 ± 0.08	18.5 ± 0.5	1.18 ± 0.05	1.91 ± 0.06

TABLE 1. Parameters of the three samples.

water film with a thickness of $\sim\Delta z$. As shown in table 1, a large α corresponds to a small separation z/a, which suggests that the local viscosity is higher when the particle monolayer in the water is farther from the water–air interface.

The water–air interface is perfectly slipping, incapable of supporting a shear stress. Such a slip boundary corresponds to a decreased particle friction (increased mobility) and decreased energy dissipation. Intuitively, the closer a Brownian particle is to the water–air interface, the less surrounding water can be driven by the particle's moving, because the water film between the particle and the interface is thinner. The particle will thus feel less viscosity when approaching the interface, unlike that in the bulk of the water. From (3.1), we can know that for a particle that is far away from the water–air interface, the particle's friction is increased with respect to its bulk value, and the diffusion constant is decreased, so the value of the measured diffuse constant tends to its bulk values.

According to the work of Sickert, Rondelez & Stone (2007) and Fischer, Dhar & Heinig (2006), the single-particle diffusion coefficient can be written as

$$D_s(n) \cong \frac{k_B T}{\kappa^{(0)}\eta^{(b)}a + \kappa^{(1)}\eta^{(s1)}(n)}, \tag{3.2}$$

where k_B is the Boltzmann constant and $\eta^{(s1)}(n)$ is the n-dependent surface viscosity of the particle monolayer. Equation (3.2) indicates that the friction of a particle experienced in a monolayer (or a film) comes from two terms: $\kappa^{(0)}\eta^{(b)}a$ and $\kappa^{(1)}\eta^{(s1)}$. The first term represents the friction due to the viscosity experienced by the particle in its local environment, where $\eta^{(b)}$ is the viscosity of the bulk of fluid and $\kappa^{(0)}$ is related to the position of the monolayer. The second term represents the friction coming from the monolayer (or film) itself, which is a function of the area fraction n. The dimensionless coefficients $\kappa^{(0)}$ and $\kappa^{(1)}$, which are the functions of z, can be calculated by following equations (Fischer *et al.* 2006),

$$\kappa^{(0)} \approx 6\pi\sqrt{\tanh\left[\frac{32(z/a+1)}{9\pi^2}\right]}, \tag{3.3}$$

$$\kappa^{(1)} \approx -4\times\ln\left(\frac{2}{\pi}\arctan\left(\frac{2}{3}\right)\right)\frac{(3a)^{3/2}}{(z+2a)^{3/2}} \quad (z \geq a). \tag{3.4}$$

The calculated values of $\kappa^{(0)}$ and $\kappa^{(1)}$ for the three samples are listed in table 1. More details about the method to obtain the values of $\kappa^{(0)}$ and $\kappa^{(1)}$ are presented in the supplementary material available at https://doi.org/10.1017/jfm.2020.693. Given the results of $D_s(n)$, the surface viscosity $\eta^{(s1)}$ of the monolayers can be estimated by (3.2). The Saffman length λ_s can be obtained by $\lambda_s = \eta^{(s1)}/\eta^{(b)}$ (Saffman & Delbrück 1975; Saffman 1976). The curves of λ_s vs. n are shown in figure 2(b), which indicates that λ_s increases with n monotonically.

The correlated diffusion reflects the response function of the HIs between two particles (Crocker *et al.* 2000; Gardel, Valentine & Weitz 2005; Prasad *et al.* 2006). In terms of the particle displacement, the correlated diffusion coefficient is defined as

$$D_{||,\perp}(r) = \frac{\langle \Delta s^i_{||,\perp}(t,\tau)\Delta s^j_{||,\perp}(t,\tau)\delta(r - R^{i,j}(t))\rangle_{i\neq j}}{2\tau}. \tag{3.5}$$

Here, $\Delta s^i_{||,\perp}$ is the displacement of the ith particle in the longitudinal ($||$) or transverse ($\perp$) direction during a time interval τ, as shown in figure 1(c). The longitudinal displacement $\Delta s_{||}$ and transverse displacement $\Delta s_\perp$ are the components of $\Delta s_i(\tau)$ that are parallel and

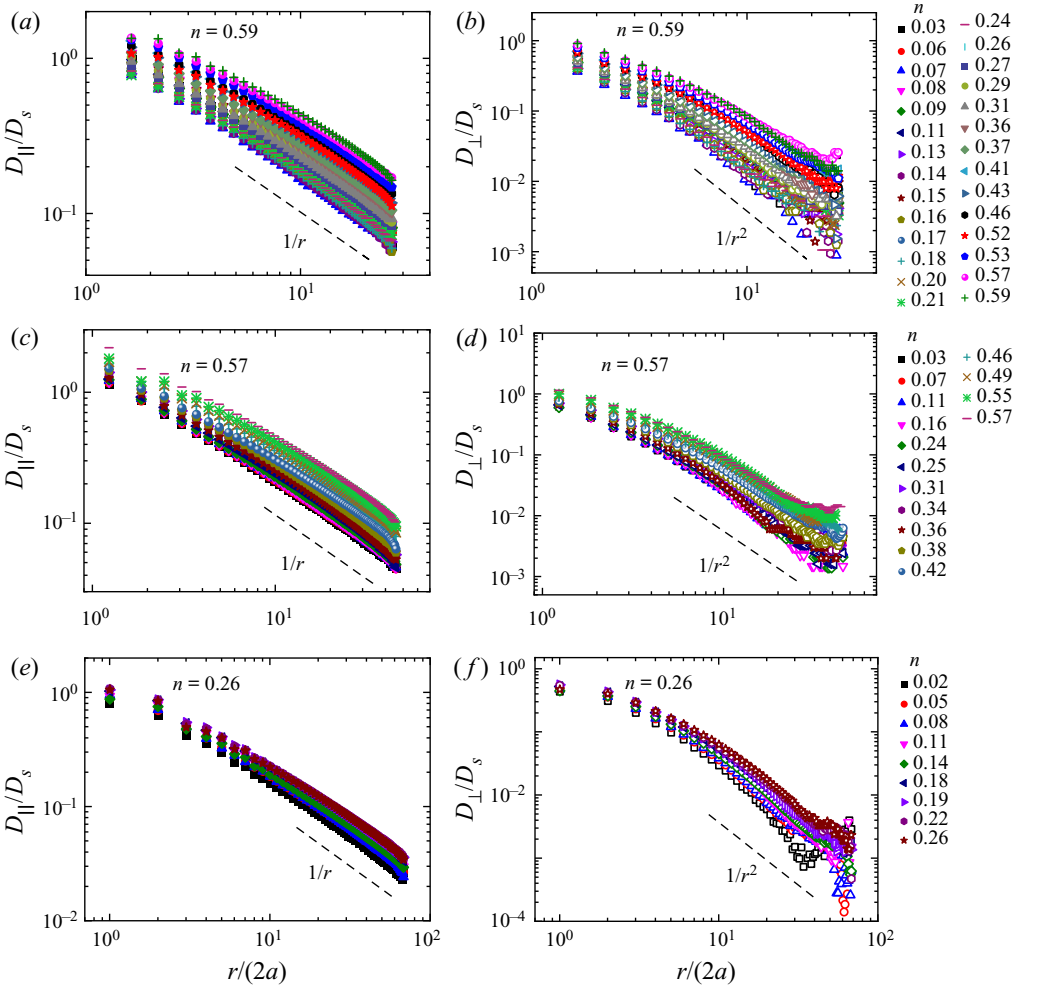

FIGURE 3. Measured correlated diffusion coefficients $D_{||}/D_s(n)$ (*a*) and $D_\perp/D_s(n)$ (*b*) as a function of the distance $r/(2a)$ for sample Si1; (*c* and *d*) for sample Si2; (*e* and *f*) for sample Si3. The different symbols represent measurements at different area fractions n. The highest n is labelled in each figure. The dashed lines corresponding to $\sim 1/r$ (*a*) and $\sim 1/r^2$ (*b*) are plotted for reference.

perpendicular, respectively, to the line connecting the centres of two particles i and j. The average $\langle\rangle_{i\neq j}$ is taken over all pairs consisting of the ith and jth particles with a separation distance r for $i \neq j$. The correlated diffusion coefficients $D_{||,\perp}(r)$ for sample Si1 are plotted in figure 3(*a*,*b*), where the results are normalized with respect to the single-particle diffusion $D_s(n)$ to eliminate the effects of the local viscosity. In figure 3(*a*,*b*), from bottom to top, the area fraction n varies from 0.03 to 0.59, and the black squares and green crosses correspond to the smallest and largest n values, respectively. The curves of $D_{||,\perp}(r)$ for samples Si2 and Si3 are plotted in figures 3(*c*,*d*) and 3(*e*,*f*), and exhibit behaviours similar to those of $D_{||\perp}(r)$ for sample Si1.

Curves of $D_{||\perp}(r)$ in figure 3(*a–f*) collapse to a single master curve $\tilde{D}_{||,\perp}(R_{||,\perp})$ for each direction when an effective diffusion coefficient D_s^m and adjustable parameters $\chi_{||,\perp}$ are

used as the scaling factors in vertical and horizontal axis respectively, i.e. $\tilde{D}_{||} \equiv D_{||}/D_s^m$ and $R_{||,\perp} \equiv r/\chi_{||,\perp}$ (see figure 4). The effective diffusion coefficient D_s^m is obtained by the single-particle diffusion coefficient $D_s(n)$ in the following method. As shown in (3.2), the retardation experienced by a Brownian particle involves two factors: the local viscosity experienced by the particle in the dilute limit $\kappa^{(0)}\eta^{(b)}a$ and the many-body effect of the particles $\kappa^{(1)}\eta^{(s)}$ in the particle monolayer. Based on (3.2), two effective diffusion coefficients can be defined by $D_s(0) \equiv k_BT/\kappa^{(0)}\eta^{(b)}a$ and $D_s^m(n) \equiv k_BT/\kappa^{(1)}\eta^{(s1)}$. Hence, (3.2) can be rewritten as

$$\frac{1}{D_s(n)} = \frac{1}{D_s(0)} + \frac{1}{D_s^m(n)}. \tag{3.6}$$

Here, $D_s(0)$ is the diffusion coefficient of a single particle in the monolayer in the dilute limit ($n \to 0$), which can be obtained from figure 2(*a*), and $D_s^m(n)$ is a function of n because the viscosity $\eta^{(s1)}$ stems from the HIs between particles in the monolayer. Since the measured correlated diffusion coefficients $D_{||,\perp}(r)$ describe the HIs between particles, $D_s^m(n)$ is a more suitable scaling factor than $D_s(n)$ for this scenario.

The scaling factors $\chi_{||,\perp}$, which are the functions of n, can be regarded as characteristic lengths of the particle monolayer. Based on the concept of the Saffman length, the values of $\chi_{||,\perp}(n)$ are determined by the ratio of the surface viscosity of the monolayer and the bulk viscosity of water (Saffman & Delbrück 1975). When $\chi_{||}(n)$ obtained in figure 4(*a*,*c*,*e*) are regarded as

$$\chi_{||} = \eta_{||}^{(s2)}/\eta^{(b)}, \tag{3.7}$$

the surface viscosity $\eta_{||}^{(s2)}$ of the monolayer can be estimated from the value of $\chi_{||}$. The comparison between such $\eta_{||}^{(s2)}$ and $\eta^{(s1)}$ is plotted in figure 5(*a*), which reads that $\eta_{||}^{(s2)}$ and $\eta^{(s1)}$ agree with each other. The values of $\eta_{||}^{(s2)}$ and $\eta^{(s1)}$, which are obtained in one-particle and two-particle measurements respectively, should agree with each other for the same homogeneous monolayer (Prasad *et al.* 2006; Zhang *et al.* 2013*b*). Usually, the agreement between $\eta_{||}^{(s2)}$ and $\eta^{(s1)}$ will be satisfied when n is small. The monolayer can turn into a heterogeneous state with an increase in n. Then, there will be a gradual deviation between $\eta_{||}^{(s2)}$ and $\eta^{(s1)}$ with an increase in n, (Prasad *et al.* 2006) as shown in figure 5(*a*). The results in figure 5(*a*) suggest that $\chi_{||}$ is the Saffman length indeed, i.e. $\chi_{||} = \lambda_s$.

However, we found that $\chi_\perp(n)$ obtained in figure 4(*b*,*d*,*f*) cannot be regarded as the Saffman length λ_s. If $\chi_\perp(n) = \lambda_s$ was regarded, the values of $\eta_\perp^{(s2)}$ estimated from $\chi_\perp(n) = \eta_\perp^{(s2)}/\eta^{(b)}$ would disagree with the values of $\eta^{(s1)}$. The comparison between such $\eta_\perp^{(s2)}$ and $\eta^{(s1)}$ is plotted in figure 5(*b*), indicating that the viscosity $\eta_\perp^{(s2)}$ obtained from $\chi_\perp = \lambda_s$ follows the power-law relationship $\eta_\perp^{(s2)} \sim (\eta^{(s1)})^{2/3}$. Considering this power-law relationship, the dependence of the scaling length $\chi_\perp$ on the Saffman length $\lambda_s = \eta_\perp^{(s2)}/\eta^{(b)}$ should be expressed as

$$\chi_\perp = \frac{1}{2}a\left(\frac{\lambda_s}{a}\right)^{2/3}, \tag{3.8}$$

for $\eta_\perp^{(s2)} = \eta^{(s1)}$ to be satisfied. The viscosity $\eta_\perp^{(s2)}$ that is obtained using (3.8) is plotted against $\eta^{(s1)}$ in figure 5(*c*). Once again, the values of $\eta^{(s1)}$ and $\eta_\perp^{(s2)}$ agree with each other when n is small. The comparison between the viscosity $\eta_{||}^{(s2)}$ and $\eta_\perp^{(s2)}$ is plotted in figure 5(*d*), which shows $\eta_{||}^{(s2)} = \eta_\perp^{(s2)}$ all the time.

It should be noted that there exist sets of values of $\chi_{||,\perp}$ and their multiples such that all of these values can make $\tilde{D}_{||,\perp}$ collapse to a single curve. However, there is only one

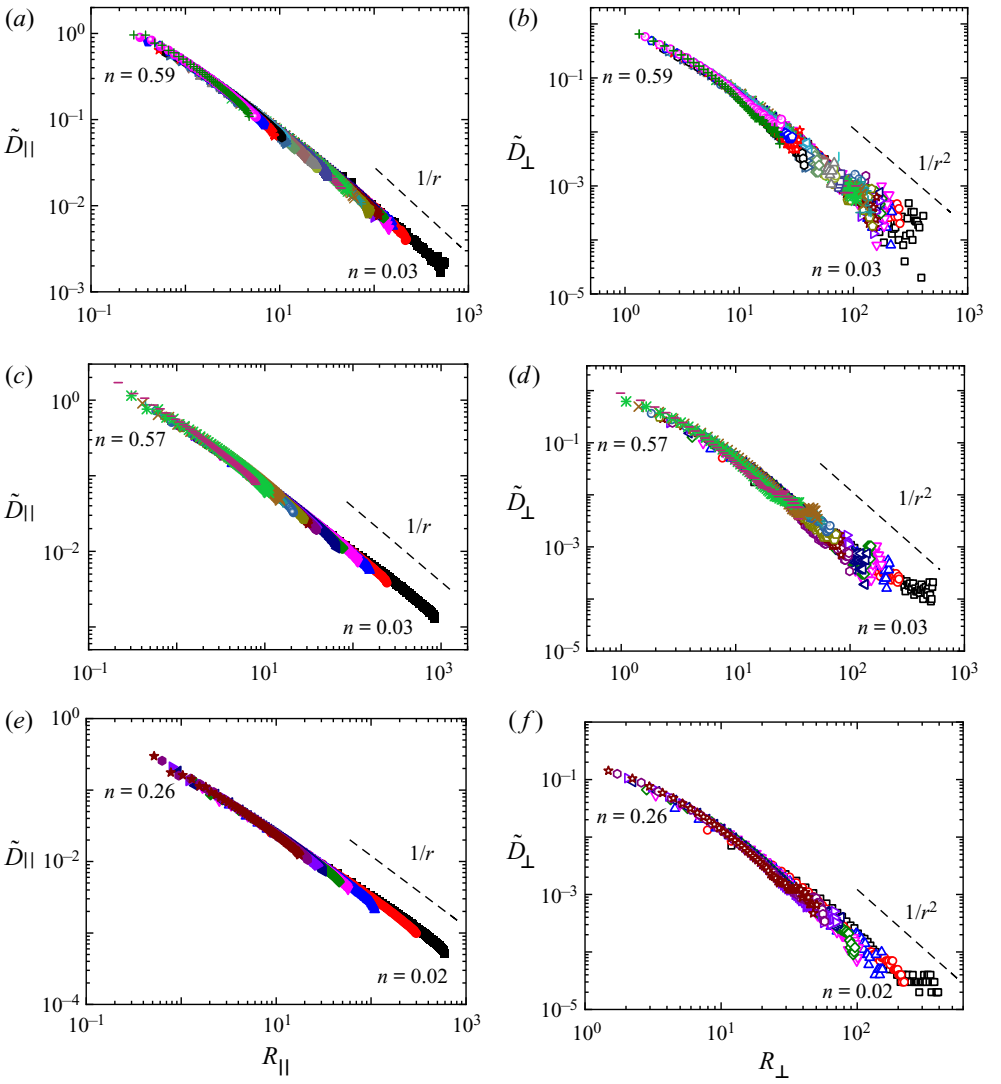

FIGURE 4. Scaled correlated diffusion coefficients $\tilde{D}_{||}(R_{||})$ (*a*) and $\tilde{D}_{\perp}(R_{\perp})$ (*b*) for sample Si1; (*c* and *d*) for sample Si2; (*e* and *f*) for sample Si3. The symbols used are same as in figure 3.

special pair of $\chi_{||,\perp}$ values for which the calculated viscosity $\eta^{(s2)} \equiv \eta^{(s2)}_{||,\perp}$ agrees with $\eta^{(s1)}$. This constraint allows for one to determine a unique pair of $\chi_{||,\,\perp}$ values with which to determine the positions of the master curves of $\tilde{D}_{||,\perp}$.

The dependence of $\eta^{(s2)}$ on n is plotted in figure 6, showing that it follows the Krieger–Dougherty equation (Krieger & Dougherty 1959) as follows:

$$\eta^{(s2)} = \eta^{(s1)}(0)\left[\left(1 - \frac{n}{n_m}\right)^{-[\eta]n_m} - 1\right], \tag{3.9}$$

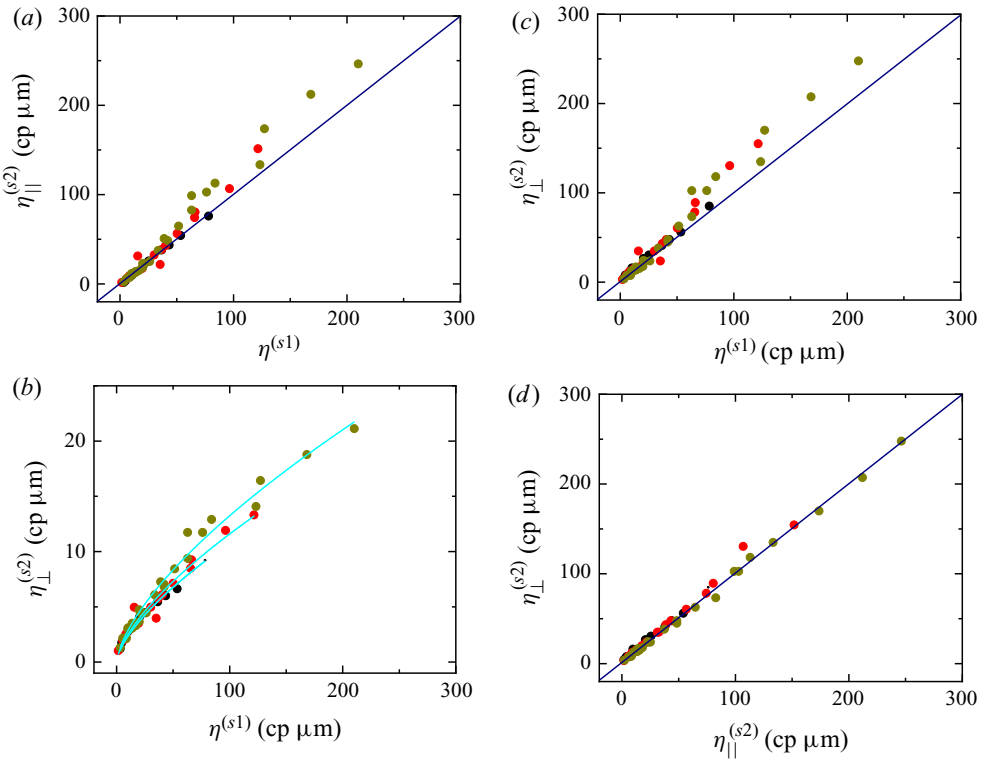

FIGURE 5. (*a*) Plots of $\eta_{||}^{(s2)}$ vs. $\eta^{(s1)}$ for three samples. (*b*) Plots of $\eta_{\perp}^{(s2)}$ vs. $\eta^{(s1)}$ calculated from $\chi_{\perp} = \lambda_s$ for three samples. The cyan curves represent fits to $\eta_{\perp}^{(s2)} \sim (\eta^{(s1)})^{2/3}$. (*c*) Plots of $\eta_{\perp}^{(s2)}$ vs. $\eta^{(s1)}$ calculated from (3.7). (*d*) Plots of $\eta_{\perp}^{(s2)}$ vs. $\eta_{||}^{(s2)}$ from (3.7) for three samples. The navy blue line in (*a*,*c*,*d*) is shown for reference, and the slope of the line is 1.0.

where $\eta^{(s1)}(0)$ is a characteristic scale for the surface viscosity, which is affected by the confining boundary. In the above equation, $n_m \cong 0.84$ is the maximum random packing fraction in two dimensions (Berryman 1983; O'Hern *et al.* 2002), and the intrinsic viscosity $[\eta]$ is the only fitting parameter. The fitted values of the intrinsic viscosity $[\eta]$ are shown in table 1.

In the vicinity of a fluid–fluid interface, the mobility of particles and the hydrodynamic interactions between particles will be different from those in the bulk, which show a complex dependence on the separation z (Jones, Felderhof & Deutch 1975; Bickel 2007; Wang *et al.* 2009, 2011*b*). In our experiments, $\tilde{D}_{||}$ and $\tilde{D}_{\perp}$ indeed depend on the separation z. The larger z is, the weaker the influence of the water–air interface. The master curves of $\tilde{D}_{||}(R_{||})$ and $\tilde{D}_{\perp}(R_{\perp})$ with different z each degenerate to a single curve when $\tilde{D}_{||}(R_{||})$ and $\tilde{D}_{\perp}(R_{\perp})$ are multiplied by a factor of $(z/a)^{2/3}$ (as shown in figure 7). This degeneracy of $\tilde{D}_{||,\perp}$ by a factor of $(z/a)^{2/3}$ at $z > 0$ indicates that, with the exception of the boundary effect, no dynamic mechanisms are introduced into the system by the water–air interface.

It can be seen from figure 7(*b*) that the value for Si3 is slightly lower than the other two. This deviation between them looks more obvious in the half-log plot (see supplementary figure S1). We think that such deviation comes from fluctuations in the vertical position of the particles, which will weaken HIs between the particles at given projection

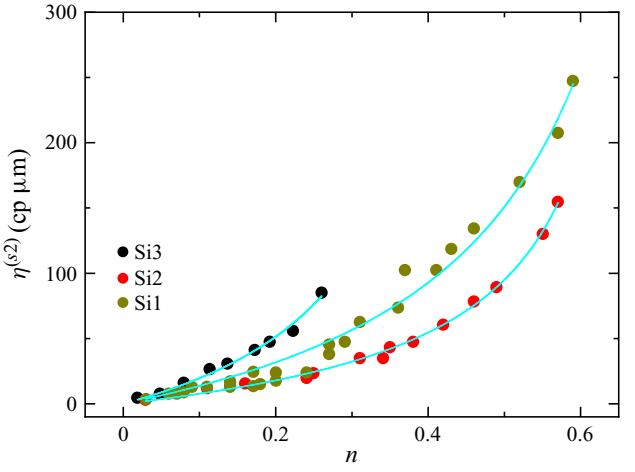

FIGURE 6. The surface viscosities $\eta^{(s2)}$ as functions of the particle area fraction n. The cyan curves represent fits to the Krieger–Dougherty equation.

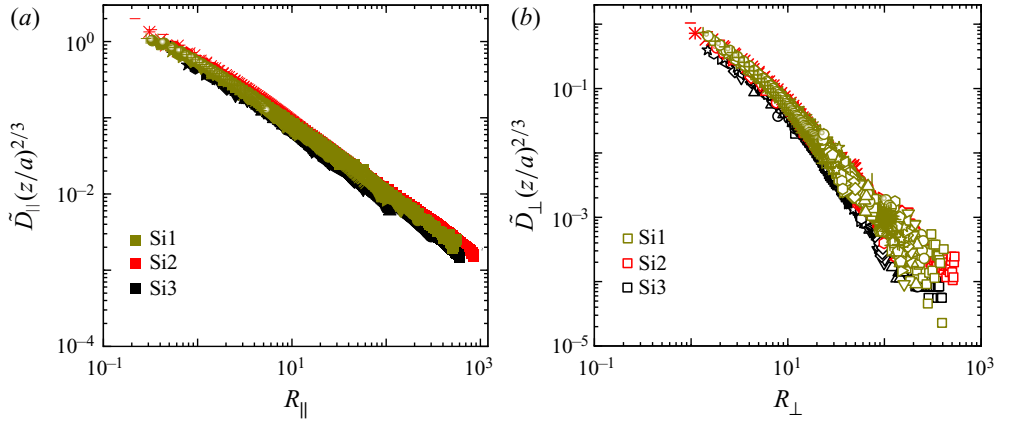

FIGURE 7. (*a*) Universal master curve of $\tilde{D}_{||}(z/a)^{2/3}$ as a function of $R_{||}$ for three samples. (*b*) Universal master curve of $\tilde{D}_{\perp}(z/a)^{2/3}$ as a function of $R_{\perp}$ for three samples.

distance r. The smaller the mass of the particles, the greater the fluctuations experienced in the vertical position. The correlated diffusion, $D_{||\perp}(r)$, of Sample Si3 was smaller than that of the other two samples. Another feature of such deviation is that a significant deviation appears in a short distance, as the strength of such an influence is supposed to be proportional to $\Delta z/r$.

4. Discussion

It should be noted that the screened Coulomb repulsive interaction exists in addition to hydrodynamic interactions between the charged particles immersed in water. However, such a Coulomb interaction is a short-range interaction, which usually occurs in few Debye screening lengths. The samples were left undisturbed for 7–8 h before the measurement. The CO_2 resolves in the DI water during this time, which increases the concentration of counterions in the water solution and reduces the Debye screening lengths to the

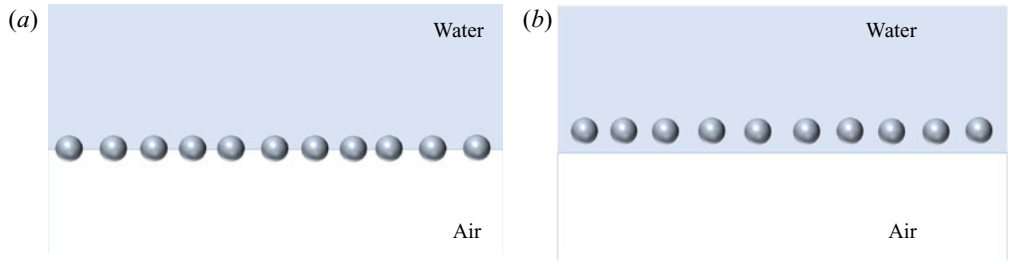

FIGURE 8. Two kinds of colloidal systems. (*a*) The particle monolayer is at the water–air interface. (*b*) The particle monolayer is near the water–air interface.

order of 0.1 μm. The measured $D_{||,\perp}(r)$ in a range of 2–30 μm in figure 3 will not be affected by such a short-range interaction. The particles totally immerse in the water and are away from the interface, which excludes the presence of capillary interaction or dipole interaction between the particles. In fact, the hydrodynamic interaction is the only long-range interaction in our system, which corresponds to the behaviours of $D_{||\perp}(r)$ obtained here.

When $r \gg \lambda_s$, one usually has $D_{||}(r) \sim 1/r$ and $D_{\perp}(r) \sim 1/r^2$ for the monolayer of particles suspended in a liquid. The particles in such a 2-D monolayer cannot conserve momentum, but diffuse momentum into the surrounding fluid, leading to the fact that the r-dependence of $D_{||,\perp}$ in the monolayer is dominated by the surrounding liquid. In the longitudinal direction, the dependence of $D_{||}(r) \sim 1/r$ is identical to the longitudinal correlation in an unbounded fluid, caused by 3-D shear stresses, while in the transverse direction, the dependence of $D_{\perp}(r) \sim 1/r^2$ arises from 2-D compressive stresses due to the force of effective dipoles. For a particle monolayer located just at the water–air interface (figure 8*a*), the scaling lengths in the longitudinal and transverse directions are identical (Prasad *et al.* 2006; Zhang *et al.* 2013*b*). In our experiments, however, the monolayer is located a short distance from the water–air interface (figure 8*b*), and the scaling lengths differ in the two directions. This phenomenon can be attributed to the boundary effect of the water–air interface. Figure 3(*a*,*c*,*e*) shows that $D_{||}(r)$ decays with r as $\sim 1/r$ in the longitudinal direction. This results from the HIs response to a 3-D-like shear stress in the bulk water and the thin-film water, which acts as a kind of semi-3-D system due to the momentum conservation in a 3-D liquid (Nägele *et al.* 1993; Crocker *et al.* 2000; Levine & Lubensky 2000; Oppenheimer & Diamant 2009, 2010). In figure 3(*b*,*d*,*f*), $D_{\perp}(r)$ decays as $\sim 1/r^2$ in the transverse direction, showing behaviour that has been attributed to long-range compression and modelled as interactions of effective mass dipoles (Cui *et al.* 2004; Shani *et al.* 2014). This difference in the variation tendencies of the correlated diffusion coefficients in the longitudinal and transverse directions is universal among colloidal monolayers suspended in fluids (Oppenheimer & Diamant 2009, 2010).

In this water–air system, the scaling length is separated into a longitudinal scaling length λ_s and a transverse scaling length $\chi_{\perp}$. Such a scaling method for r can also be applied in a similar way to the water–oil system. The relationship between them follows $2\chi_{\perp}/a = (\lambda_s/a)^{2/3}$. This relationship may be understood by comparison with that of the lubrication of a liquid film confined between two solid surfaces. The normal load capacity of the film depends on the form of hydrodynamic action that the film experiences (Hamrock, Schmid & Jacobson 2004). In the case of squeezing action, the normal load capacity is $W_{squeeze} = (w'/\eta^{(b)}u_{squeeze})(h_{squeeze}/l)^3$, where w', $u_{squeeze}$, $h_{squeeze}$, and l are the normal load per unit

length, squeezing velocity, film thickness and length of the solid surface, respectively. Similarly, the expression for the load capacity for sliding action (Hamrock *et al.* 2004) is $W_{sliding} = (w'/(\eta^{(b)}u_{sliding}))(h_{sliding}/l)^2$, where $h_{sliding}$ is the thickness of the liquid film and $u_{sliding}$ is the sliding velocity. When these two load capacities are comparable (i.e. $W_{squeeze} \sim W_{sliding}$) with $u_{squeeze} = u_{sliding}$, the equation $h_{squeeze}/l \sim (h_{sliding}/l)^{2/3}$ is obtained, with a functional form similar to that of $2\chi_\perp/a = (\lambda_s/a)^{2/3}$. This analogy is based on the recognition that the squeezing and sliding actions for a confined film are equivalent to the compression and shear stress between the particles in a particle monolayer (Oppenheimer & Diamant 2009, 2010). Thus, the relationship between the two scaling lengths of the particle monolayer has the same form as that of $h_{squeeze}/l = (h_{sliding}/l)^{2/3}$.

The form of the scaling length $\chi_\perp = a(\lambda_s/a)^{2/3}/2$ can also be understood by analogy to lubrication theory. The squeezing force between two particles of radius a with a separation distance r in a liquid is $f = \xi(r)U$, where U is the velocity at which one particle is approaching the other and $\xi(r)$ is the hydrodynamic friction coefficient. When the two particles are suspended in a 3-D liquid with a separation distance r_{3D}, the friction coefficient is $\xi(r_{3D}) = (3/2)\pi\eta^{(b)}a(a/r_{3D})$ (Russel, Saville & Schowalter 1992). In a 2-D system, such as two circular disks of radius a with a separation distance r_{2D} approaching each other in a thin liquid film (Hamrock *et al.* 2004), the friction coefficient of the squeezing force is $\xi(r_{2D}) = (3/2)\pi\eta_s(a/r_{2D})^{3/2}$. Here, the viscosity of the film, η_s, is equal to $\eta^{(b)}a$. By equating these two kinds of squeezing lubrication forces [i.e. $\xi(r_{2D}) = \xi(r_{3D})$], we find that $r_{2D} = a(r_{3D}/a)^{2/3}$, which is similar to $\chi_\perp = a(\lambda_s/a)^{2/3}/2$.

5. Conclusions

In this work, for a particle monolayer near a water–air interface, the correlated diffusion coefficients of the particles in the longitudinal and transverse directions are presented in the form of normalized functions $\tilde{D}_{\parallel,\perp}(R_{\parallel,\perp})$. From such correlated diffusion measurements, the longitudinal scaling length is the Saffman length λ_s of the particle monolayer, and the transverse scaling length $\chi_\perp$ follows a power-law relationship with λ_s, as expressed by $\chi_\perp = a(\lambda_s/a)^{2/3}/2$. Using these scaling lengths, the master curves of the correlated diffusion and viscosity of such particle monolayers can be obtained. Studies of the correlated diffusion of a colloidal monolayer near a water–oil interface have been reported previously (Zhang *et al.* 2013*a*). Data collapse into master curves was achieved by a phenomenological scaling method, which does not improve our understanding. Compared with the previous results, the scaling lengths in this work provide a better way to understand the collapse of correlated diffusion curves. Using the scaling method described here, the surface viscosities of monolayers can be calculated correctly. Our experiments provide a set of reliable data that can be used for the further development of theoretical models to study the dynamics of liquids near soft interfaces.

Acknowledgements

This research is supported by the National Natural Science Foundation of China (Grant Nos. 11474054, 11774417 and 11604381), and the Natural Science Foundation of Jiangsu Province (Grant No. BK20160238).

Declaration of interests

The authors report no conflict of interest.

Supplementary material

Supplementary material is available at https://doi.org/10.1017/jfm.2020.693.

REFERENCES

BEGAM, N., CHANDRAN, S., SPRUNG, M. & BASU, J. K. 2015 Anomalous viscosity reduction and hydrodynamic interactions of polymeric nanocolloids in polymers. *Macromolecules* **48** (18), 6646–6651.

BERRYMAN, J. G. 1983 Random close packing of hard-spheres and disks. *Phys. Rev.* A **27** (2), 1053–1061.

BICKEL, T. 2007 Hindered mobility of a particle near a soft interface. *Phys. Rev.* E **75**, 041403.

CAI, L. H., PANYUKOV, S. & RUBINSTEIN, M. 2011 Mobility of nonsticky nanoparticles in polymer liquids. *Macromolecules* **44** (19), 7853–7863.

CARUSO, F., GRIESER, F., MURPHY, A., THISTLETHWAITE, P., URQUHART, R., ALMGREN, M. & WISTUS, E. 1991 Determination of lateral diffusion-coefficients in air water monolayers by fluorescence quenching measurements. *J. Am. Chem. Soc.* **113** (13), 4838–4843.

CHEN, W. & TONG, P. 2008 Short-time self-diffusion of weakly charged silica spheres at aqueous interfaces. *Europhys. Lett.* **84** (2), 28003.

CROCKER, J., VALENTINE, M., WEEKS, E., GISLER, T., KAPLAN, P., YODH, A. G. & WEITZ, D. 2000 Two-point microrheology of inhomogeneous soft materials. *Phys. Rev. Lett.* **85**, 888–891.

CUI, B., DIAMANT, H., LIN, B. & RICE, S. A. 2004 Anomalous hydrodynamic interaction in a quasi-two-dimensional suspension. *Phys. Rev. Lett.* **92** (25), 258301.

DI LEONARDO, R., KEEN, S., IANNI, F., LEACH, J., PADGETT, M. J. & RUOCCO, G. 2008 Hydrodynamic interactions in two dimensions. *Phys. Rev.* E **78** (3), 031406.

DI RIENZO, C., PIAZZA, V., GRATTON, E., BELTRAM, F. & CARDARELLI, F. 2014 Probing short-range protein Brownian motion in the cytoplasm of living cells. *Nat. Commun.* **5** (1), 5891.

DUFRESNE, E., SQUIRES, T., BRENNER, M. & GRIER, D. 2000 Hydrodynamic coupling of two Brownian spheres to a planar surface. *Phys. Rev. Lett.* **85**, 3317–3320.

FISCHER, T. M., DHAR, P. & HEINIG, P. 2006 The viscous drag of spheres and filaments moving in membranes or monolayers. *J. Fluid Mech.* **558**, 451–475.

FRYDEL, D. & DIAMANT, H. 2010 Long-range dynamic correlations in confined suspensions. *Phys. Rev. Lett.* **104**, 248302.

GARDEL, M. L., VALENTINE, M. T. & WEITZ, D. A. 2005 *Microscale Diagnostic Techniques*. Springer.

HAMROCK, B. J., SCHMID, S. R. & JACOBSON, B. O. 2004 *Fundamentals of Fluid Film Lubrication*. Marcei Dekker.

HE, W., SONG, H., SU, Y., GENG, L., ACKERSON, B. J., PENG, H. B. & TONG, P. 2016 Dynamic heterogeneity and non-Gaussian statistics for acetylcholine receptors on live cell membrane. *Nat. Commun.* **7** (1), 11701.

HUANG, K. & SZLUFARSKA, I. 2015 Effect of interfaces on the nearby Brownian motion. *Nat. Commun.* **6** (1), 8558.

HUANG, S., GAWLITZA, K., VON KLITZING, R., STEFFEN, W. & AUERNHAMMER, G. K. 2017 Structure and rheology of microgel monolayers at the water/oil interface. *Macromolecules* **50** (9), 3680–3689.

JONES, R. B., FELDERHOF, B. U. & DEUTCH, J. M. 1975 Diffusion of polymers along a fluid-fluid interface. *Macromolecules* **8** (5), 680–684.

KRIEGER, I. M. & DOUGHERTY, T. J. 1959 A mechanism for non-Newtonian flow in suspensions of rigid spheres. *Trans. Soc. Rheol.* **3** (1), 137–152.

LEVINE, A. & LUBENSKY, T. 2000 One- and two-particle microrheology. *Phys. Rev. Lett.* **85**, 1774–1777.

MCWHIRTER, J. L., NOGUCHI, H. & GOMPPER, G. 2009 Flow-induced clustering and alignment of vesicles and red blood cells in microcapillaries. *Proc. Natl Acad. Sci. USA* **106** (15), 6039–6043.

MISIUNAS, K., PAGLIARA, S., LAUGA, E., LISTER, J. R. & KEYSER, U. F. 2015 Nondecaying hydrodynamic interactions along narrow channels. *Phys. Rev. Lett.* **115** (3), 038301.

NÄGELE, G., KELLERBAUER, O., KRAUSE, R. & KLEIN, R. 1993 Hydrodynamic effects in polydisperse charged colloidal suspensions at short times. *Phys. Rev.* E **47** (4), 2562–2574.

O'Hern, C. S., Langer, S. A., Liu, A. J. & Nagel, S. R. 2002 Random packings of frictionless particles. *Phys. Rev. Lett.* **88** (7), 075507.

Oppenheimer, N. & Diamant, H. 2009 Correlated diffusion of membrane proteins and their effect on membrane viscosity. *Biophys. J.* **96** (8), 3041–3049.

Oppenheimer, N. & Diamant, H. 2010 Correlated dynamics of inclusions in a supported membrane. *Phys. Rev.* E **82** (4), 041912.

Ouali, L. & Pefferkorn, E. 1996 Hydrodynamic thickness of interfacial layers obtained by adsorption of a charged diblock copolymer on a selective surface from aqueous solutions. *Macromolecules* **29** (2), 686–692.

Parigi, G., Rezaei-Ghaleh, N., Giachetti, A., Becker, S., Fernandez, C., Blackledge, M., Griesinger, C., Zweckstetter, M. & Luchinat, C. 2014 Long-range correlated dynamics in intrinsically disordered proteins. *J. Am. Chem. Soc.* **136** (46), 16201–16209.

Park, B. J. & Lee, D. 2015 Dynamically tuning particle interactions and assemblies at soft interfaces: reversible order-disorder transitions in 2D particle monolayers. *Small* **11** (35), 4560–4567.

Prasad, V., Koehler, S. A. & Weeks, E. R. 2006 Two-particle microrheology of quasi-2D viscous systems. *Phys. Rev. Lett.* **97** (17), 176001.

Ramadurai, S., Holt, A., Krasnikov, V., van den Bogaart, G., Killian, J. A. & Poolman, B. 2009 Lateral diffusion of membrane proteins. *J. Am. Chem. Soc.* **131** (35), 12650–12656.

Russel, W. B., Saville, D. A. & Schowalter, W. R. 1992 *Colloidal Dispersions*. Cambridge University Press.

Saffman, P. G. 1976 Brownian-motion in thin sheets of viscous-fluid. *J. Fluid Mech.* **73**, 593–602.

Saffman, P. G. & Delbrück, M. 1975 Brownian motion in biological membranes. *Proc. Natl Acad. Sci. USA* **72** (8), 3111–3113.

Shani, I., Beatus, T., Bar-Ziv, R. H. & Tlusty, T. 2014 Long-range orientational order in two-dimensional microfluidic dipoles. *Nat. Phys.* **10** (2), 140–144.

Sickert, M., Rondelez, F. & Stone, H. A. 2007 Single-particle Brownian dynamics for characterizing the rheology of fluid Langmuir monolayers. *Europhys. Lett.* **79** (6), 66005.

Vivek, S. & Weeks, E. R. 2015 Measuring and overcoming limits of the Saffman-Delbruck model for soap film viscosities. *PLoS ONE* **10** (3), e0121981.

Wang, C.-J., Ackerman, D. M., Slowing, I. I. & Evans, J. W. 2014 Langevin and Fokker-Planck analyses of inhibited molecular passing processes controlling transport and reactivity in nanoporous materials. *Phys. Rev. Lett.* **113** (3), 038301.

Wang, D., Yordanov, S., Paroor, H. M., Mukhopadhyay, A., Li, C. Y., Butt, H. J. & Koynov, K. 2011*a* Probing diffusion of single nanoparticles at water-oil interfaces. *Small* **7** (24), 3502–3507.

Wang, G., Prabhakar, R. & Sevick, E. 2009 Hydrodynamic mobility of an optically trapped colloidal particle near fluid-fluid interfaces. *Phys. Rev. Lett.* **103**, 248303.

Wang, G. M., Prabhakar, R., Gao, Y. X. & Sevick, E. M. 2011*b* Micro-rheology near fluid interfaces. *J. Opt.* **13** (4), 044009.

Wille, A., Valmont, F., Zahn, K. & Maret, G. 2002 Shear modulus of two-dimensional colloidal crystals. *Europhys. Lett.* **57** (2), 219–225.

Zhang, W., Chen, S., Li, N., Zhang, J. & Chen, W. 2013*a* Universal scaling of correlated diffusion of colloidal particles near a liquid-liquid interface. *Appl. Phys. Lett.* **103** (15), 154102.

Zhang, W., Li, N., Bohinc, K., Tong, P. & Chen, W. 2013*b* Universal scaling of correlated diffusion in colloidal monolayers. *Phys. Rev. Lett.* **111** (16), 168304.